Isotope mass and charge effects in tokamak plasmas

I. Pusztai,[1] J. Candy,[2] and P. Gohil[2]
[1]*Department of Applied Physics, Nuclear Engineering, Chalmers University of Technology and Euratom-VR Association, SE-41296 Göteborg, Sweden*
[2]*General Atomics, P.O. Box 85608, San Diego, California 92186-5608, USA*

(Received 24 February 2011; accepted 27 October 2011; published online 13 December 2011)

The effect of primary ion species of differing charge and mass—specifically, deuterium, hydrogen, and helium—on instabilities and transport is studied in DIII-D plasmas through gyrokinetic simulations with GYRO [J. Candy and E. Belli, General Atomics Technical Report No. GA-A26818, 2010]. In linear simulations under imposed similarity of the profiles, there is an isomorphism between the linear growth rates of hydrogen isotopes, but the growth rates are higher for $Z > 1$ main ions due to the appearance of the charge in the Poisson equation. On ion scales the most significant effect of the different electron-to-ion mass ratio appears through collisions stabilizing trapped electron modes. In nonlinear simulations, significant favorable deviations from pure gyro-Bohm scaling are found due to electron-to-ion mass ratio effects and collisions. The presence of any non-trace impurity species cannot be neglected in a comprehensive simulation of the transport; including carbon impurity in the simulations caused a dramatic reduction of energy fluxes. The transport in the analyzed deuterium and helium discharges could be well reproduced in gyrokinetic and gyrofluid simulations while the significant hydrogen discrepancy is the subject of ongoing investigation. [doi:10.1063/1.3663844]

I. INTRODUCTION AND MOTIVATION

Although the fundamental aspects of thermal confinement in tokamak core plasmas are reasonably well understood in terms of transport due to drift-wave turbulence, the more subtle details of *isotope scaling* are less-well understood. In particular, the experimentally observed favorable scaling of confinement time with isotope mass remains an unresolved problem.

The bulk part of the turbulent energy transport in tokamak cores usually comes from ion scale fluctuations ($k_y\rho_{si} \sim 1$) with frequencies comparable to c_{si}/a, where k_y is the binormal wave number, $c_{si} = \sqrt{T_e/m_i}$ is the ion sound speed, $\rho_{si} = c_{si}/\Omega_{ci}$ is the ion sound Larmor radius, $\Omega_{ci} = Z_i eB/(m_i c)$ is the cyclotron frequency, Z_i is the ion charge of species i, a is the minor radius of the plasma. It is expected that for different main ion species the turbulence remains similar except that typical lengths and frequencies are changed according to the charge and mass scalings of the sound speed and Larmor radius. If this was the case, dimensional considerations suggest that the diffusivities should exhibit gyro-Bohm scaling,

$$\chi_{\mathrm{gB}i} \doteq \rho_{si}^2 \frac{c_{si}}{a} = \frac{\sqrt{A_i}}{Z_i^2}\rho_s^2 \frac{c_s}{a}, \tag{1}$$

where $A_i = m_i/m$ for an ion with the mass m_i and the species subscript i is suppressed for deuterium ions, which is the nominal primary ion in tokamak plasmas. This implies that for hydrogen isotopes the energy confinement time τ_E should decrease with increasing isotope mass according to $\tau_E \sim a^2/\chi_{\mathrm{gB}} \propto A_i^{-1/2}$ when the temperature is kept constant, or $\tau_E \propto A_i^{-1/5}$ for fixed power $P \sim nTa^3/\tau_E$. On the contrary, an abundance of experimental evidence in various confinement modes shows that the energy confinement usually increases as one moves from hydrogen to deuterium or deuterium-tritium (DT) plasmas.[1–4] However, the mass scaling is found to be varying in a wide range $A_i^{0-0.85}$,[3] strongly depending on the operating modes.

There have been several models proposed to explain the experimentally found deviation from the gyro-Bohm scaling. The decreasing trend of ion temperature gradient (ITG) mode growth rates with isotope mass, found in linear simulations with adiabatic electron response, could explain a favorable mass scaling of the confinement time, assuming that the radial correlation length of the fluctuations is independent of ion Larmor radius, as argued in Ref. 5 by Dong *et al.* Bateman[6] suggests that the increase in the edge temperatures with isotope mass might account for favorable isotope scaling. Tokar[7] found that by applying an improved mixing length estimate to dissipative trapped electron (TE) mode turbulence, a favorable scaling with isotope mass may be realized. However, this model fails to demonstrate empirical scaling with other parameters as argued by Waltz.[8] In other work, the role of $E \times B$ shear stabilization due to the equilibrium (neoclassical) radial electric field was explored by Ernst *et al.*[9] The model of Ref. 9—based on gyrofluid and gyrokinetic simulations with trapped electrons and sheared flows included in an approximate way—predicted a varying isotopic mass scaling and was shown to agree closely with D-T experiments on TFTR. In local nonlinear gyrokinetic simulations for the ITG dominated collisionless GA standard case,[10] Estrada-Mila *et al.* found practically no deviation from gyro-Bohm scaling[11] for D, T, and DT plasmas. Ultimately, a commonly accepted and robust theoretical explanation of the isotope effect which is consistent with the other experimentally established parameter scalings is lacking.

In the present paper, we aim to study the effect of primary ion species of differing charge and mass—specifically, deuterium, hydrogen, and helium—on instabilities and transport. To this end, first-principles non-linear gyrokinetic simulations are carried out with GYRO (Refs. 12 and 13), based on experimental plasma profiles and magnetic geometry from a series of DIII-D L-mode discharges.

The paper is organized as follows. We start with the description of the chosen discharges and data processing in Sec. II, then linear and nonlinear similarity simulations based on the deuterium discharge are discussed in Secs. III and IV, respectively. Finally, in Sec. V, we present the transport analysis of the different discharges and compare non-linear GYRO simulations to the experiments. The results are summarized in Sec. IV.

II. OVERVIEW OF TARGET DIII-D L-MODE DISCHARGES

We chose L-mode phases from three balanced neutral beam injection (NBI) DIII-D discharges which have different main ion species: deuterium (129135, 1250–1300 ms), hydrogen (133778, 1225–1275 ms), and helium (138767, 2700–2750 ms). The balanced injection yields approximately zero net torque, thereby minimizing the effect of rotation and rotation shear in these plasmas. We emphasize that these were not similarity experiments; that is, the plasma profiles are somewhat different in each of the three discharges as shown in Fig. 1 However, the discharges are similar in several aspects. When viewed from above in these lower single-null plasmas, the orientation of the magnetic field ($B \sim 2\,\mathrm{T}$) was clockwise, whereas the plasma current ($I_p \sim 1$ MA) was counter-clockwise in all cases; this is the standard configuration on DIII-D. Electron cyclotron resonance heating (ECRH) and NBI were the auxiliary heating methods applied. The dominant impurity in these discharges is carbon, and the hydrogen and helium plasmas contained a considerable amount of deuterium minority ions.

The experimental data were collected from the MDSplus database[14] of General Atomics and pre-processed by the tools ONETWO (Ref. 15) for the deuterium and hydrogen discharges and by TRANSP (Refs. 16 and 17) for the non-standard helium discharge (as non-hydrogenic main species is not supported by ONETWO). We note that a TRANSP analysis of the hydrogen discharge gave results quite similar to the ONETWO analysis presented here. The rotation profiles used in the non-linear simulations were calculated using a tool based on the neoclassical code NEO (Ref. 18), which first calculates the radial electric field by matching the neoclassical toroidal rotation of carbon at the outboard-midplane with the measured values then recomputes the poloidal and toroidal flows for all species.

III. LINEAR SIMULATIONS UNDER IMPOSED SIMILARITY

To separate charge and mass effects from the effects due to differences in the plasma parameter profiles in the three discharges, in the following two sections the GYRO simulations presented are based on plasma parameter profiles from the deuterium discharge. We refer to these simulations as *similarity studies*. The only parameters changed in the simulations are the ion charge and mass (also, in the helium case the ion density is scaled for quasineutrality). We move from the simplest model to more and more sophisticated and realistic simulations. In order to understand how turbulent transport is affected by charge and mass effects, it is instructive to analyze the underlying instabilities. We performed local linear gyrokinetic simulations with GYRO where flows and the impurity content are neglected. The local shape and profile parameters,

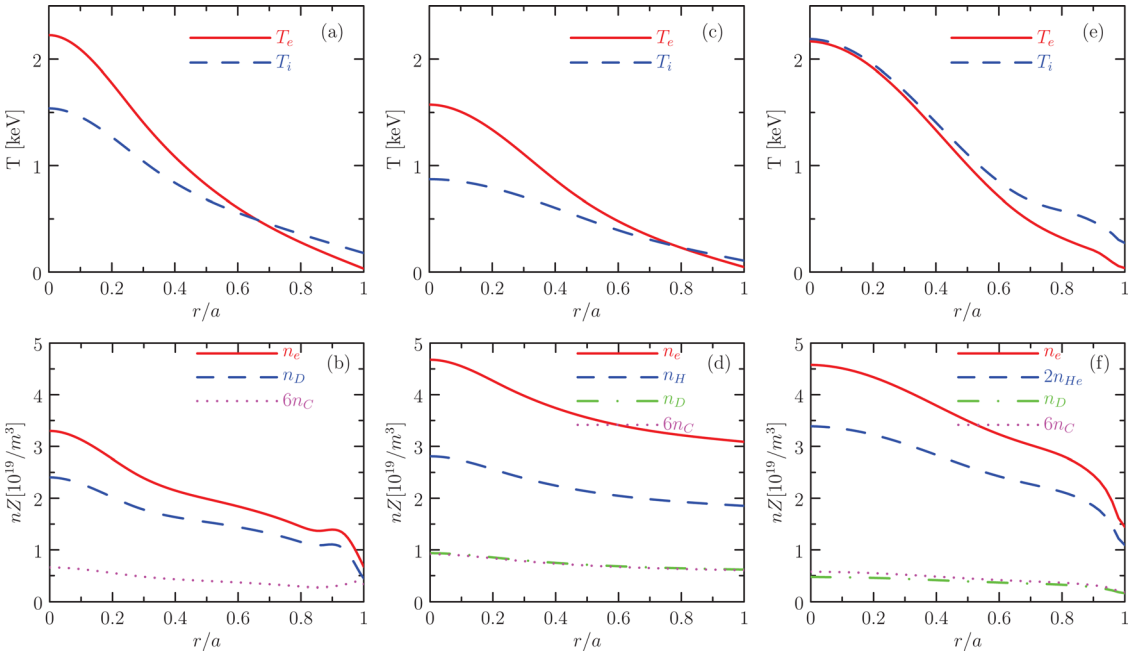

FIG. 1. (Color online) Temperature and density profiles for the deuterium (a) and (b), hydrogen (c) and (d), and helium (e) and (f) discharges. For ions, the density profiles are multiplied by the ion charge.

following the notation defined in Ref. 19, for $r/a=0.55$ are the following: $R_0/a=2.88$, $q=1.78$, $s=0.75$, $\kappa=1.34$, $\delta=0.107$, $\rho_s/a=1.03\times10^{-3}$, $a/L_n=-a(d\ln n_e/dr)=0.68$, $a/L_{Ti}=-a(d\ln T_i/dr)=1.89$, $a/L_{Te}=-a(d\ln T_e/dr)=2.69$, and $(a/c_s)\nu_{ei}=0.143$.

First, we consider a purely adiabatic electron response and neglect ion-ion collisions; in this case the electron-to-ion mass ratio and collisional effects cannot play a role. In a pure plasma with adiabatic electrons, we expect to find only toroidal ion temperature gradient modes characterized by typical frequencies ω_r and growth rates γ comparable to the magnetic drift frequencies $k_\theta\rho_{si}(c_{si}/R)$, where k_θ is the poloidal wave number and R is the major radius. Henceforth, $c_s=c_{s\mathrm{D}}$ and $\rho_s=\rho_{s\mathrm{D}}$ are understood. The linearized collisionless ion gyrokinetic equation[20] for the non-adiabatic part of the perturbed ion distribution g_i can be written as

$$i\sqrt{\frac{2}{\tau}}\frac{ax_\parallel}{Rq}\frac{\partial g_i}{\partial\theta}+\left(\frac{\omega}{c_{si}/a}-k_\theta\rho_{si}\omega_D\right)g_i = \frac{Z_ien_i\phi e^{-x^2}J_0(z_i)}{T_i\left(c_{si}\sqrt{2\pi/\tau}\right)^3}\left(\frac{\omega}{c_{si}/a}-k_\theta\rho_{si}\omega_*^T\right), \quad (2)$$

where $\omega_D=-2a/(R\tau)(x_\perp^2/2+x_\parallel^2)(\cos\theta+s\theta\sin\theta)$, $\omega_*^T=-a/(L_{ni}\tau)[1+(x^2-3/2)L_{ni}/L_{Ti}]$, τ is the electron-to-ion temperature ratio, q is the safety factor, s is the magnetic shear, θ is the extended poloidal angle, $x=v/v_i$ is the velocity normalized to the thermal speed $v_i=\sqrt{2T_i/m_i}$, n_i and T_i are the ion density and temperature, ϕ is the perturbed potential, ω is the mode frequency, J_0 is the Bessel function of the first kind and $z_i=k_\perp\rho_{si}\sqrt{2/\tau}$.

Noting that $Z_in_i=n_e$ for a pure plasma, we find that Eq. (2) depends on the ion mass and charge only through c_{si} and ρ_{si}. The naive expectation is that if we normalize the wave numbers and frequencies to the species units so that ρ_{si} and c_{si} are calculated for the ion species in question, then we should find identical $\gamma(k_y\rho_{si})$ curves where γ is given in c_{si}/a units and k_y is the binormal wave number.

In Fig. 2, ITG growth rates found in similarity studies at $r/a=0.55$ are plotted against binormal wave number in both deuterium units (red curves) and species units (blue curves with markers for H and He), i.e., the sound speed and Larmor radius used in the normalization are those for the ion species. The hydrogen and deuterium plasmas obey our expectation; that is, their growth rates in species units are identical, (red solid curve and blue dashed curve), see Fig. 2(a). We note that $\rho_{s\mathrm{H}}=\rho_{s\mathrm{He}}=\rho_s/\sqrt{2}$ and $c_{s\mathrm{H}}/\sqrt{2}=c_s=c_{s\mathrm{He}}\sqrt{2}$; the $1/\sqrt{m_i}$ dependence of the frequencies (in absolute units) in hydrogen isotope plasmas is consistent with the findings of Ref. 5. However, the helium growth rate in species units (blue dotted curve) in Fig. 2(b) is considerably higher than that for deuterium, although the wave number corresponding to its maximum approximately coincides with that for the other species.

The higher growth rates for helium arise from the explicit appearance of the charge in the Poisson equation and can be understood by considering the effect of the helium charge on the dispersion relation. The latter follows from the Poisson equation (quasineutrality) applied to the perturbed electron and ion densities $\tilde{n}_e=Z_i\tilde{n}_i$. In Appendix A, it is illustrated that ITG growth rates in the long wavelength limit scale roughly as $Z_i^{1/2}$ in species units, clarifying the scaling observed in Fig. 2(b).

As a next step, we consider non-adiabatic electron response in the linear similarity studies, still neglecting collisions. In this case the toroidal ITG growth rates become somewhat higher as shown in Fig. 3(a). We remark that the destabilizing effect of non-adiabatic electrons on ITG is well known. It is more interesting to note that now the isomorphism between hydrogen and deuterium growth rates (normalized to species units) is not perfect anymore, the hydrogen growth rate being slightly higher. Although the difference is small, with the symmetry-breaking characterized by the parameter $\sqrt{m_e/m_i}$. This observation is consistent with the frequent observation that, in GK simulations, an artificially decreased mass-ratio usually increases the linear growth rates and transport. As the magnetic and diamagnetic drift frequencies do not depend on mass (for fixed temperature), there are only two points in the collisionless linear electrostatic electron GK equation where mass ratio differences can appear; one is $J_0(k_\perp\rho_e)$, which plays a role only on spatial scales as small as $k_\perp\sim1/\rho_e$, the other is the parallel streaming term $\mathbf{v}_\parallel\cdot\nabla g_e$. For trapped electrons (giving the main contribution to the non-adiabatic electron response),

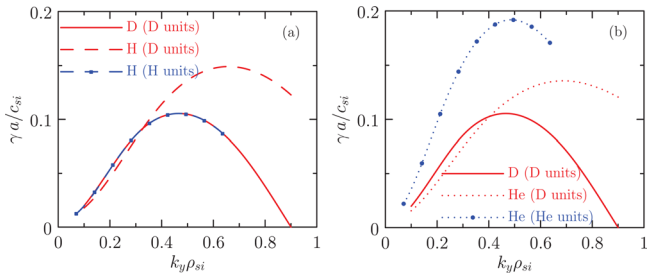

FIG. 2. (Color online) Growth rates from linear GYRO simulations with adiabatic electrons for pure deuterium (solid curve), hydrogen (dashed curve), and helium (dotted curve) plasmas, based on parameters taken from the deuterium discharge at $r/a=0.55$. Only the toroidal ITG mode is unstable in each case. Curves without markers show results normalized to fixed deuterium units, whereas the curves with markers show the results rescaled to the given species units.

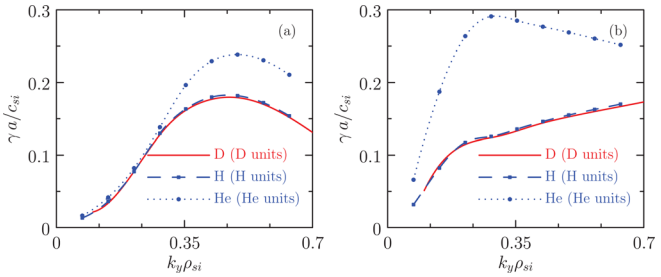

FIG. 3. (Color online) Growth rates from linear GYRO simulations with kinetic electrons (but without collisions) for pure deuterium (solid curve), hydrogen (dashed curve), and helium (dotted curve) plasmas, based on parameters taken from the deuterium discharge at $r/a=0.55$. Both ITG mode (a) and TE mode (b) roots are plotted. Curves without markers show results normalized to fixed deuterium units, whereas the curves with markers show the results rescaled to the given species units.

this term vanishes on orbit average. For this reason, the mass-ratio effect must come from the nearly adiabatic circulating electrons and therefore is rather small.

With non-adiabatic electrons in the absence of collisions, a new unstable root—a trapped electron mode—appears; the corresponding growth rates are shown in Fig. 3(b). As the TE and ITG growth rates are of similar magnitude, these simulations were performed using the *Maxwell dispersion matrix eigenvalue solver* method[21] in GYRO, which is capable of finding sub-dominant eigenmodes. Once again, the growth rates for deuterium and hydrogen in species units nearly (but not exactly) coincide. The TE growth rate for helium is not only higher than expected, but exhibits a qualitatively different behavior from the two hydrogen isotopes for higher wave numbers: it decreases with increasing wave number. We note—without including a corresponding figure—that the ITG and TE modes do not merge for low wave numbers; the sign of their real frequencies remains different as $k_y\rho_s \to 0$.

Including electron-ion collisions (see Fig. 4) leads to two notable differences. First, the difference in the ITG growth rates between the two hydrogen isotopes becomes larger due to the dependence of the electron-ion collision frequency ν_{ei} on the electron mass (ν_{ei} is the same in absolute units but different in species units). The other more important difference is that collisions stabilize the TE modes; for deuterium and helium, there is no unstable TE mode in the $k_y\rho_{si}$ region plotted here. For hydrogen, the collisional stabilization is not as strong: an unstable TE mode appears above $k_y\rho_{s\mathrm{H}} \approx 0.45$ (blue dashed line in the lower right corner of Fig. 4). The weaker collisional stabilization for hydrogen compared to deuterium is due to the $1/\sqrt{m_e}$ dependence of the electron-ion collision frequency, recalling that the hydrogen plasma is *similar* to a deuterium plasma with an artificially low value of $\sqrt{m_i/m_e}$. If TE modes are present—even sub-dominantly—this effect can contribute to a favorable deviation from gyro-Bohm scaling for hydrogen isotope plasmas.

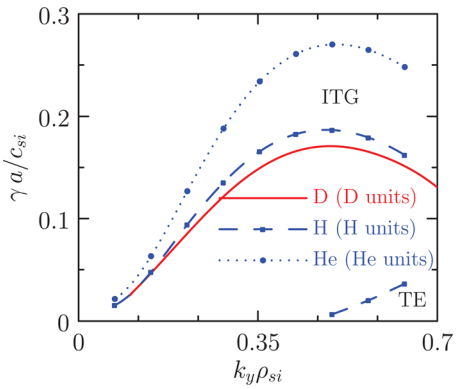

FIG. 4. (Color online) Growth rates from linear GYRO simulations with kinetic electrons and electron-ion collisions for pure plasma, based on parameters taken from the deuterium discharge at $r/a = 0.55$. In the deuterium and the helium plasmas only ITG modes are unstable for these values of $k_y\rho_s$, in the hydrogen plasma the TE mode is unstable for $k_y\rho_s > 0.65$. Curves without markers show results normalized to fixed deuterium units, whereas the curves with markers show the results rescaled to the given species units.

IV. NONLINEAR SIMULATIONS UNDER IMPOSED SIMILARITY

In this section, we present local (i.e., periodic radial boundary conditions) nonlinear similarity studies using GYRO simulations based on the data from the deuterium discharge. We change only the plasma composition—the main species and the impurities—from case to case, keeping the profiles and the geometry fixed. In these simulations, the plasma rotation is ignored since there is no sensible way to translate the rotation velocities from deuterium to the other species. Furthermore, the rotation in these cases is weak (at the diamagnetic level), whereas the rotation formulation[22] is asymptotically correct (i.e., the rotation terms are the same order as the other terms retained in the gyrokinetic equation) only if the toroidal rotation velocity is on the order of the ion thermal velocity.

The electrostatic nonlinear GYRO simulation for the deuterium case used a perpendicular domain size of $(L_x/\rho_s, L_y/\rho_s) = (107, 106)$, with the highest resolved binormal wave number $k_y\rho_s = 1.36$. The $k_x\rho_s = 0.06$–2.91 range of radial wave numbers was covered. The perpendicular resolution was adopted to the Larmor radius of the main species, keeping the number of toroidal modes fixed; the simulations covered $1/9^{\mathrm{th}}$ of the torus toroidally for deuterium, $1/13^{\mathrm{th}}[\approx 1/(9\sqrt{2})]$ for hydrogen and helium, and $1/7^{\mathrm{th}}[\approx 1/(9\sqrt{2/3})]$ for tritium. The electrons were taken to be drift kinetic with $\sqrt{m_{\mathrm{D}}/m_e} = 60$, electron-ion collisions were taken into account by an energy-dependent Lorentz operator, and the standard 128-point velocity space grid was used (8 energies, 8 pitch angles and two signs of velocity). To obtain good statistics, the cases were run above $t = 1000\, a/c_s$ with the integration time step $\Delta t = 0.01\, a/c_s$.

First, we consider the effect of kinetic electron response and collisions on transport in pure hydrogen isotope plasmas. In Fig. 5, ion (a)–(d) and electron (e) and (f) energy flux spectra from nonlinear GYRO simulations are shown for adiabatic electrons (a) and (b) and for kinetic electrons with electron-ion collisions (c)–(f). The curves represent the distribution of energy flux over poloidal wave numbers; the $k_\theta\rho_{si}$ integral of the curves gives the energy fluxes in gyro-Bohm units $\left[Q_{GBi} = n_e T_e c_{si}(\rho_{si}/a)^2 \propto m_i^{1/2}/Z_i^2\right]$. The corresponding flux values are given in the legends of the plots. The upper figures (a), (c), and (e) are normalized to fixed (deuterium) units, while the lower figures are normalized to species units. In case of purely gyro-Bohm scaling of the fluxes, the species units curves for different main species should be identical. In the local limit ($[\rho_* \doteq]\rho_{si}/a \to 0$) for pure hydrogen plasma with adiabatic electrons one should expect pure gyro-Bohm scaling, since the same normalized equations are solved and there are no mass-ratio effects breaking the similarity. The small deviations from perfect gyro-Bohm scaling in the adiabatic electron simulations shown in Fig. 5(b) are partly due to finite ρ_* effects and partly due to the limited spectral resolution of the simulations. Including kinetic electron response and collisions leads to a considerable favorable deviation from pure gyro-Bohm scaling moving from the hydrogen [dashed curves in Figs. 5(d) and 5(f)] to the deuterium (solid curves) case. However, moving from deuterium to tritium

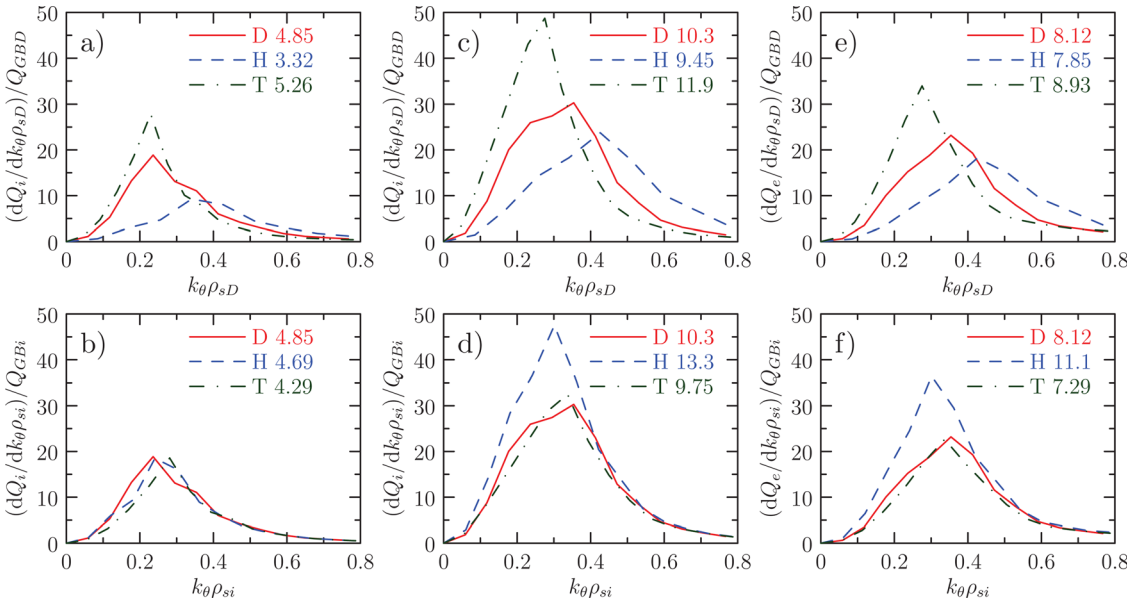

FIG. 5. (Color online) Ion (a)–(d) and electron (e) and (f) energy flux spectra from nonlinear GYRO simulations for hydrogen isotopes based on parameters taken from the deuterium discharge at $r/a = 0.65$. (a) and (b): with adiabatic electrons; (c)-(f): with kinetic electrons and electron-ion collisions. Figures (a), (c), and (e) are normalized to deuterium units, figures (b), (d), and (f) are normalized to species units.

(dashed-dotted curves) we find almost perfect gyro-Bohm scaling. The main reason for this is that the electron-to-ion mass ratio effects get saturated with increasing ion mass. Also, it might be that there are sub-dominant TE modes in the hydrogen plasma, which are already stabilized by collisions in the deuterium plasma (similar to what was found in the linear simulations with collisions in Sec. III), and there is no space for further improvement in this respect moving from deuterium to tritium.

The effect of impurities on transport in hydrogen isotope plasmas is illustrated in Fig. 6 comparing the electron energy flux spectra for pure hydrogen and deuterium plasmas (solid and dashed curves, respectively, in figures (a) and (b)) to that in hydrogen plasma with deuterium minority (dashed-dotted curve in figures (a) and (b)) $[n_D/(n_H + n_D) = 0.25]$ and to plasmas with carbon impurity (c) and (d) ($Z_{eff} = 2$). We emphasize that the species units figures are normalized to the sound speed and Larmor radius of the main ion species, even if impurities are present.

Including carbon reduces energy transport considerably, the electron channel dropping to roughly 60%–65% compared to the pure plasma cases. Without including a corresponding figure we note that the ion channel is even more affected; the total ion energy flux is reduced to 50%. The stabilizing effect of carbon impurity can also be seen in linear simulations (as it was recently reported in Ref. 23, and prior to this in Ref. 5), however the reduction of linear growth rates is not as strong as the reduction of the fluxes in nonlinear simulations. We note that interpolation formulas for the ion heat diffusivity based on nonlinear gyrofluid simulations with adiabatic electrons, presented in Ref. 24, also show reduced transport with increasing carbon concentration above an effective ion charge of $Z_{eff} = 3$.

Introducing deuterium in the hydrogen plasma somewhat decreases the transport if there is no carbon present as it is shown in Fig. 6(b), comparing the H and H + D cases. This is counter-intuitive, since one might expect that having deuterium in a hydrogen plasma brings the transport closer to that in a deuterium plasma in absolute units, which would mean increase in the transport. However, if there is carbon present, the transport is approximately the same with and without deuterium minority. It is worth pointing out that the energy transport in absolute units in the deuterium plasma with carbon impurity is almost the same as that in a hydrogen plasma with deuterium and carbon impurities, although

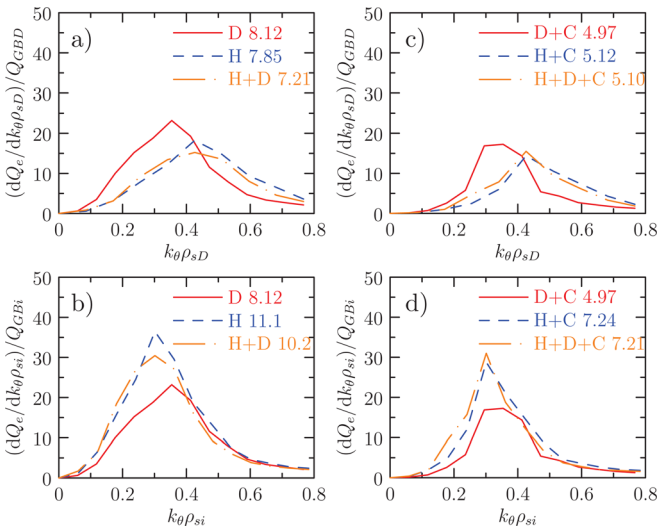

FIG. 6. (Color online) Electron energy flux spectra from nonlinear GYRO simulations for pure and impure hydrogen and deuterium plasmas based on parameters taken from the deuterium discharge at $r/a = 0.65$. (a) and (b): without carbon; (c) and (d): with carbon. Deuterium minority is included in the H + D and H + D + C cases (dashed-dotted curve). Figures (a) and (c) are normalized to deuterium units, figures (b) and (d) are normalized to species units.

the shape of their energy flux spectra is different. This is a strong favorable deviation from pure gyro-Bohm scaling which predicts $1/\sqrt{2}$ times lower transport in the hydrogen plasma, although it is too weak to explain the experimentally observed favorable mass scaling in itself.

In Sec. III, we found that species units linear growth rates of ITG and TE modes are higher in helium than in hydrogen isotope plasmas. Accordingly, the energy transport in species units is also higher in helium plasmas, as can be seen by comparing the He (dotted) and D (solid) curves and corresponding flux values in Figs. 7(b) and 7(d). For example the electron energy flux in the pure helium plasma is almost twice as high as in the pure deuterium plasma. On the ion energy transport channel the effect of higher growth rates is partly balanced by the lower ion density, so the species units ion energy flux is only 30% higher in helium than in deuterium plasma. If there is no deuterium minority in the helium plasma, including carbon impurity reduces somewhat the energy fluxes, but not as strongly as for hydrogen isotopes; see the dotted curves of Figs. 7(d) and 7(f). On the other hand, if there is deuterium minority present in the helium plasma, carbon does not reduce the transport (long dashed curves in figures (d) and (f)). Comparing the He (dotted) to the He + D (dashed) lines of Figs. 7(b) and 7(d), one finds that similarly to hydrogen plasmas, including deuterium minority—without carbon—does not increase transport in helium plasmas. While gyro-Bohm scaling would predict that the transport should be $1/(2\sqrt{2})$ times lower for helium than for deuterium in absolute units, we find that in a realistic ion composition helium plasma the energy transport is approximately the same as in an impure deuterium plasma [He + D + C and D + C curves, respectively, in Fig. 7(e)].

V. NONLINEAR GYRO SIMULATIONS FOR DIFFERENT RADII

After the similarity studies using the same plasma parameter profiles, we now turn to the actual experimental data for all the three chosen discharges and make an attempt to reproduce the electron and ion heat transport in these cases with nonlinear GYRO simulations. The local nonlinear simulations were performed at three radii, $r/a = 0.45$, 0.55, 0.65. The difference with regard to the settings of the GYRO simulations discussed in the beginning of Sec. IV is that in these simulations neoclassical flows are included for all species. The toroidal mode number separation was decreased for the cases $r/a = 0.45$ and 0.55, in order to keep the central box size and the wave number resolution approximately the same as at $r/a = 0.65$.

From experimental energy source and heat exchange profiles and magnetic geometry, the energy flux profiles are calculated by the TGYRO (Ref. 25) code in MW/m^2. The fluxes are then converted to deuterium gyro-Bohm units using the plasma parameter profiles; the conversion means a division by a radially varying factor proportional to $n_e T_e^{5/2}$. Finally, the neoclassical fluxes calculated by NEO are subtracted to obtain the "experimental" (or "target") turbulent energy fluxes.

The experimental electron and ion energy fluxes are plotted with dashed lines in Fig. 8 for the three discharges. The upper figures (a) and (b) are normalized to deuterium gyro-Bohm units, and the lower ones (c) and (d) are in SI units. The filled markers joined by solid lines represent the nonlinear GYRO simulations. The triangle markers (red curves) correspond to the deuterium, the circle markers (blue curves) to the hydrogen and the square markers (green curves) to the helium discharge. The local shape and profile

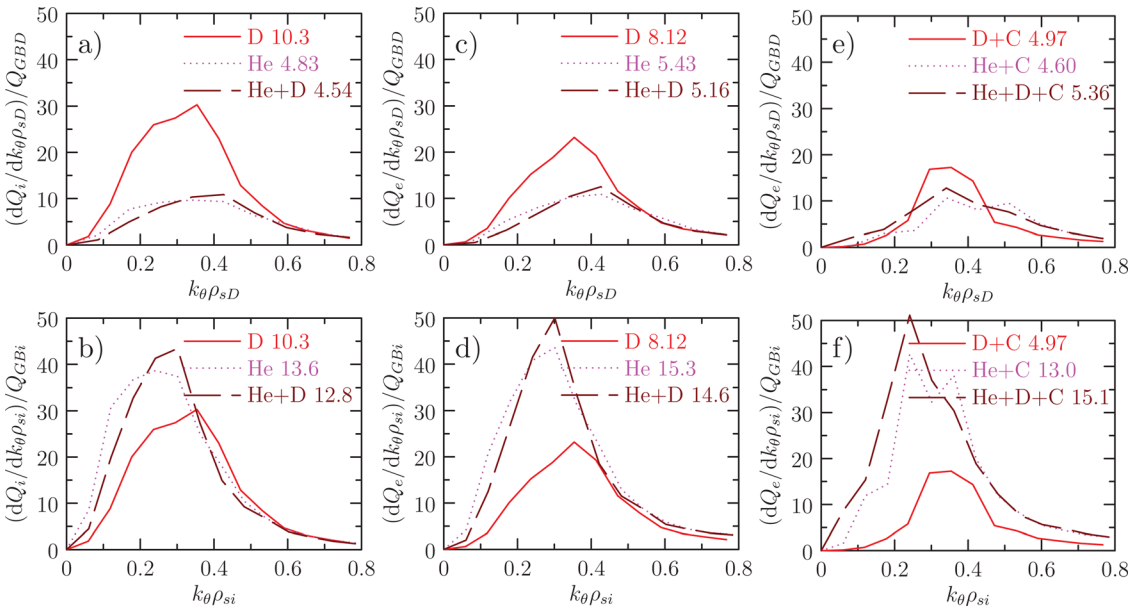

FIG. 7. (Color online) Ion (a) and (b) and electron (c)–(f) energy flux spectra from nonlinear GYRO simulations for pure and impure deuterium and helium plasmas based on parameters taken from the deuterium discharge at $r/a = 0.65$. (a)–(d): Without carbon; (e) and (f): with carbon. Deuterium minority is included in the He + D and He + D + C cases (dashed curve) $[n_D/(n_{He} + n_D) = 0.25]$. Figures (a), (c), and (e) are normalized to deuterium units, figures (b), (d), and (f) are normalized to species units.

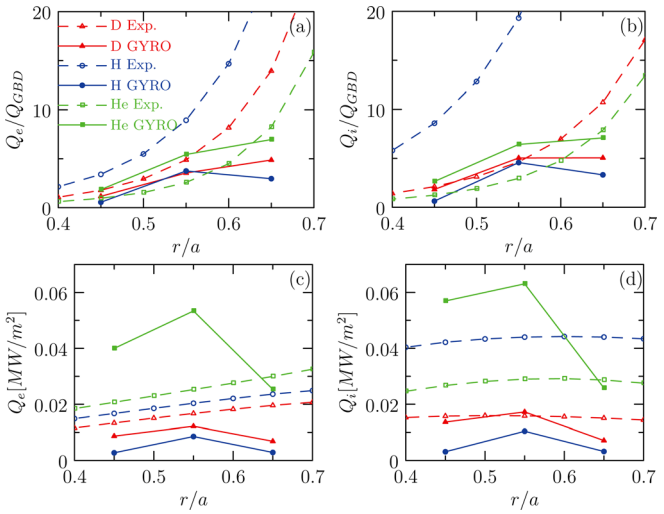

FIG. 8. (Color online) Electron (a) and (c) and ion (b) and (d) energy fluxes in deuterium gyro-Bohm units (a) and (b) and in MW/m^2 (c) and (d). The experimental (power balance) fluxes are plotted with dashed curves and open symbols, the full symbols (joined by solid curves) are nonlinear GYRO simulations. Deuterium discharge: triangle markers, hydrogen discharge: circle markers, helium discharge: square markers.

parameters at the reference radii are listed in Table I for the three discharges.

The SI unit experimental fluxes are roughly constant over the studied radial range (see the dashed lines in the lower plots of Fig. 8), which implies that the gyro-Bohm fluxes increase rapidly towards the edge (dashed lines in the upper plots) due to the decreasing electron density and temperature. As it is usually observed, gyrokinetic turbulence simulations fail to reproduce this strongly increasing trend of gyro-Bohm fluxes. Apart from this known shortcoming of gyrokinetic models, which affects the GYRO simulations in the outermost simulation points, the general increasing trend of the gyro-Bohm fluxes is reproduced by GYRO.

The GYRO simulations can be most easily related to the results of Sec. IV in gyro-Bohm units, see Figs. 8(a) and 8(b). Consistently with the similarity simulations, we find that for a given discharge the GYRO predictions for electron and ion energy fluxes are comparable. Also, GYRO predicts the gyro-Bohm fluxes in the deuterium and hydrogen discharges to be comparable, being somewhat higher in the deuterium plasma. However, we find that the transport in the helium plasma is predicted to be higher than in the hydrogen isotope plasmas, although, according to the similarity simulations we should expect similar level of gyro-Bohm fluxes in the helium and deuterium cases. This shows that the differences in the profiles cannot be disregarded.

In the experiments, the gyro-Bohm fluxes are similar for deuterium and helium, being somewhat higher in the deuterium discharge, while they are the highest in the hydrogen plasma. In particular, the ion energy flux is exceptionally high for hydrogen compared to the two other discharges. The conversion factor between gyro-Bohm and SI units fluxes $n_e T_e^{5/2}$ is 0.7 times lower in the hydrogen and 2.4 times higher in the helium than in the deuterium discharge on average in the studied radial region. Accordingly, while the GYRO predictions for the hydrogen isotope plasmas are similar in gyro-Bohm units, the predicted energy flux in MW/m^2 is the lowest for the hydrogen discharge. The experimental energy fluxes are the lowest in the Helium discharge in gyro-Bohm units, but in SI units they are the lowest in the deuterium discharge.

In general, there is a reasonably good agreement between experiments and GYRO predictions in the helium plasma and we find quite good agreement in the deuterium case. But in the hydrogen case the agreement is rather poor; the high level of experimental fluxes could not be reproduced in GYRO simulations, especially the ion energy flux, which is strongly underestimated by GYRO. It is known that energy fluxes from gyrokinetic simulations are rather sensitive to changes in the temperature gradients, which is the reason for the stiffness of temperature profiles in fusion experiments. Thus, it is sensible to ask whether the discrepancy between the measured and simulated fluxes in the hydrogen discharge is due to uncertainties in the profiles. This possibility was tested by performing predictive TGYRO-TGLF/NEO simulations for the different cases, to obtain temperature profiles which would be necessary to reproduce the experimental level of energy fluxes. Since this is an iterative method requiring a large number of evaluation of transport fluxes at several radii, we used TGLF (Refs. 26 and 27) simulations instead of computationally expensive nonlinear GYRO simulations. We note that in these experimental cases TGLF and nonlinear GYRO simulations give quite similar predictions for fluxes, therefore we would not expect significantly different profiles even if GYRO simulations were used in the predictive TGYRO iteration.

In Fig. 9, the result of the tgyro profile predictions are compared to the experimental temperature profiles for the

TABLE I. Local shape and profile parameters at the three reference radii for the deuterium, hydrogen, and helium discharges.

	r/a	q	s	κ	δ	a/L_n	a/L_{Ti}	a/L_{Te}	T_i/T_e	ν_{ei}
D	0.45	1.58	0.48	1.32	0.08	0.80	1.92	2.44	0.77	0.09
	0.55	1.78	0.75	1.34	0.11	0.68	1.89	2.69	0.82	0.14
	0.65	2.08	1.10	1.36	0.14	0.79	1.94	3.07	0.91	0.23
H	0.45	1.67	0.41	1.34	0.11	0.65	1.89	2.69	0.63	0.27
	0.55	1.86	0.65	1.36	0.13	0.48	2.41	3.19	0.68	0.46
	0.65	2.12	0.98	1.38	0.17	0.33	2.28	3.56	0.76	0.84
He	0.45	1.60	0.45	1.33	0.08	0.73	1.98	2.26	1.05	0.11
	0.55	1.79	0.70	1.35	0.11	0.76	2.40	2.93	1.10	0.17
	0.65	2.07	1.06	1.37	0.14	0.72	2.59	3.63	1.18	0.30

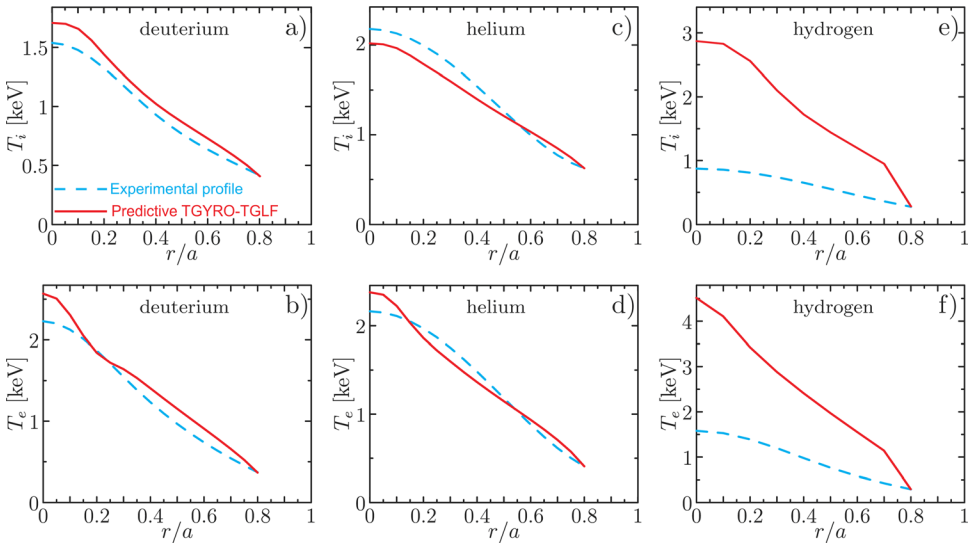

FIG. 9. (Color online) Comparison of ion and electron temperature profiles from predictive TGYRO-TGLF/NEO simulations (solid curves) to experimental profiles (dashed curves). Deuterium discharge (a) and (b), helium discharge (c) and (d), hydrogen discharge (e) and (f).

three discharges. For the deuterium and helium discharges, quite good agreement between the predicted and experimental profiles is found, thus it can be argued that the energy transport in these experiments can be explained by neoclassical transport and drift wave turbulence. However, in the hydrogen case, to get the experimental level of fluxes from these models, much steeper temperature profiles are required; in particular, the central electron and ion temperatures should be three times as high as the experimental values. (Note that steeper temperature profiles increase the transport fluxes in two ways; the stronger drive for the microinstabilities leads to higher fluxes in gyro-Bohm units, and the conversion factor between gyro-Bohm and SI unit fluxes is also higher for higher temperatures).

In the hydrogen isotope plasmas carbon impurity has a stabilizing effect as it was demonstrated in Sec. IV; another possible source of the discrepancy in the hydrogen case can be the uncertainty in the carbon concentration. This possibility was tested in simulations based on the conservative assumption of zero carbon concentration (corresponding to the highest turbulent energy transport). Without including corresponding figures we note that even in this case the predicted temperature profiles were still much steeper than in the experiments. Also, the large energy transport in the hydrogen discharge could not been reproduced even without collisions or accounting for energetic ions coming from the neutral beam injection. Finally, the possibility that the energy source profiles provided by the ONETWO analysis are erroneous were ruled out by performing similar transport analysis with TRANSP leading to similar results (see a comparison of the integrated powers in Fig. 10).

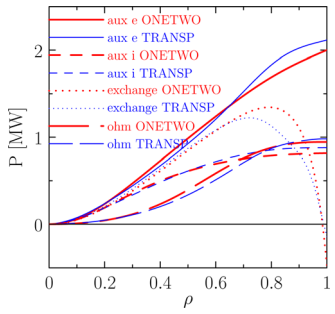

FIG. 10. (Color online) Comparison of the most important integrated powers in the hydrogen discharge from the ONETWO (thick lines) and the TRANSP (thin lines) analyses. Solid/dashed lines: auxiliary heating of electrons/ions, dotted lines: electron-ion heat exchange, long dashed lines: ohmic heating. The radiated power (not plotted) is less than 15% of the ohmic power, and the levels of charge exchange and ionization powers are even lower.

We performed several checks of the measured data, especially in the hydrogen discharge and found no obvious extraordinary property of the discharge or circumstance, that could account for the "anomalous" behavior. A comparison of the measured and calculated plasma stored energies in the three plasmas was one of the checks, with reassuring result. Here, we list the stored energy values for the three discharges in units of 0.1 MJ in the format (measured $\pm$ uncertainty, calculated): deuterium (1.35 ± 0.1, 1.44), hydrogen (1.55 ± 0.05, 1.51), helium (1.8 ± 0.1, 1.88). The hydrogen discharge was free of macroscopic MHD activity around the analyzed time slice. We also note that the experimental fluxes were similarly underestimated by TGLF for an L-mode time slice from a similar hydrogen discharge (133779).

VI. CONCLUSIONS

In the present article, we study the effect of primary ion species of differing charge and mass on drift wave instabilities and transport driven by them. We present gyrokinetic simulations of a wide range of sophistication from local linear electrostatic simulations with adiabatic electron response to non-linear simulations including several ion species and neoclassical flows. These GYRO simulations are based on experimental plasma profiles and magnetic geometry from a series of relevant L-mode discharges in the DIII-D tokamak (with hydrogen, deuterium, and helium as main ion species).

First we show simulations under imposed similarity, so that the only difference between the simulations is the ion mass and charge. Since the linearized collisionless ion gyrokinetic equation depends on these two parameters only through the ion sound speed and Larmor radius, the ITG growth rates normalized to species units for adiabatic

electron response are the same for hydrogenic ions, however if $Z > 1$, as for helium, the appearance of charge in the Poisson equation leads to higher linear growth rates. Considering the non-adiabatic electron response leads to the breaking of the perfect similarity of the growth rates between the ions with same charge due to the difference in the parallel motion of the nearly adiabatic circulating electrons. On the other hand, new unstable modes can appear such as TE mode, where like for ITG, similarity is found between the growth rates of the hydrogen isotopes, but for ions with different charge qualitative difference appears in the wave number dependence of the growth rates for higher wave numbers. By including electron-ion collisions in the linear simulations, the difference between the ITG growth rates for hydrogenic ions is further increased, and the TE mode is strongly stabilized. For the parameters we studied we found unstable growth rates only for the hydrogen, as the stabilization [which should be $\propto \nu_{ei}/(c_{si}/a)$ in species units] is the smallest for this species.

In nonlinear simulations under imposed similarity, when realistic effects such as collisions and impurities are taken into account, there can be considerable deviations from perfect gyro-Bohm scaling of the transport which is guaranteed only in the $\rho_* \to 0$ limit for pure plasmas with adiabatic electron response. With kinetic electrons and collisions, moving from hydrogen to deuterium a favorable deviation from gyro-Bohm scaling is found, while moving from deuterium to tritium the transport exhibits almost perfect gyro-Bohm scaling due to the saturation of electron-to-ion mass ratio effects and stabilization of sub-dominant modes. Including carbon in the simulations leads to a dramatic reduction of the energy fluxes in the hydrogen isotope plasmas, although the linear stabilizing effect of carbon is moderate. Deuterium minority in the hydrogen plasma can also reduce the transport, while naively the opposite trend is expected. Therefore in any comprehensive transport simulation all non-trace impurity species should be taken into account. For helium, the energy transport in species gyro-Bohm units is considerably higher than that for deuterium due to the higher linear growth rates in helium. Carbon has weaker stabilizing effect in helium than in hydrogen isotope plasmas. Including all impurities and collisions, the energy transport in a hydrogen or helium plasma can be approximately the same as in a deuterium plasma, which is a strong deviation from gyro-Bohm scaling (predicting $1/\sqrt{2}$ times lower transport in hydrogen and $1/(2\sqrt{2})$ times lower transport in helium plasma). However, this deviation in the hydrogen case is still not sufficient to explain any strong favorable mass scaling of the global energy confinement time.

Finally the similarity of the discharges was relaxed, and the actual plasma profiles were used. With these nonlinear GYRO simulations taking neoclassical flows into account, the experimental energy transport in the helium discharge can be reasonably well reproduced, while for the deuterium discharge we find even better agreement. The minor differences can be due to uncertainties in the profiles and plasma composition which plays an important role in these discharges. Also, ion and electron temperature profiles calculated by predictive TGYRO-TGLF/NEO transport simulations are quite similar to the experimental profiles for these discharges. On the other hand, the exceptionally high gyro-Bohm energy transport in the hydrogen discharge could not be reproduced by GYRO. The discrepancy is likely not due to uncertainties in the profiles as much steeper temperature profiles were necessary in predictive TGYRO-TGLF/NEO simulations to reproduce the experimentally found high level of fluxes. Further tests excluded inaccurate plasma composition, the effect of energetic ions or erroneous energy source profiles as possible sources of the discrepancy. The only notable differences between the hydrogen and the other two discharges—apart from the different main species—are that it had the lowest temperature and the highest ion density. It is not certain if the discrepancy between gyrokinetic/gyrofluid models and experiments in this discharge is related to the previously observed shortfall of gyrokinetic models towards the edge[28]. The anomalously large energy transport in the hydrogen discharge is subject of ongoing investigation and is the basis of future validation work.

ACKNOWLEDGMENTS

We thank G. Staebler for providing the TGLF model, and E. Belli for NEO support. This work was funded by the European Communities under Association Contract between EURATOM and Vetenskapsrådet and by the U.S. DOE under Contract Nos. DE-FG03-95ER54309 and DE-FG02-07ER54917 as part of the FACETS SciDAC project and used the resources of the NCCS at ORNL under Contract No. DEAC05-00OR22725. The first author is very grateful to Chalmerska Forskningsfonden and Adlerbertska Forskningsstiftelsen for their financial support, and to the Fusion Group at GA for supporting his research visits and for providing a stimulating atmosphere.

APPENDIX A: CHARGE DEPENDENCE OF LINEAR GROWTH RATES

As an illustration, we show how $Z_i \neq 1$ affects the ITG growth rate through a simplified example. The adiabatic electron response means that $\tilde{n}_e = en_e\phi/T_e$, and the perturbed ion density is given by $\tilde{n}_i = -en_e\phi\tau/T_e + \int d^3v J_0(z_i) g_i$ which depends on the ion charge and mass through c_{si} and ρ_{si} only. We neglect the finite Larmor radius (FLR) effects $J_0(z_i) \to 1$ and the parallel ion compressibility, the first term in Eq. (2). Furthermore, we use the constant energy resonance approximation $[x_\perp^2 + 2x_\parallel^2 \to 4x^2/3]$ and expand in the smallness of the magnetic drift frequency (often referred as the "non-resonant expansion"), and considering the strongly ballooning limit by taking the ion gyrokinetic equation at $\theta = 0$ we find that the dispersion relation is of the form,

$$\frac{1}{\tau Z_i} = -\frac{\omega_{*i}}{\omega} + \frac{3}{2}\frac{\omega_{di}}{\omega}\left[1 - \frac{\omega_{*i}}{\omega}\left(1 + \frac{L_{ni}}{L_{Ti}}\right)\right], \tag{A1}$$

where $\omega_{di} = -k_\theta \rho_{si} c_{si} 4/(3R\tau)$ and $\omega_{*i} = -k_\theta \rho_{si} c_{si}/(L_{ni}\tau)$. For pure plasma $L_{ni} = L_{ne} = L_n$, and equal ion and electron temperatures $\tau = 1$ (and $L_{Ti} = L_{Te} = L_T$), in the flat density $L_n/L_T \to \infty$ limit we find that the growth rate of the ITG mode is

$$\gamma \sim \left(Z_i \omega_{*i} \omega_{di} \frac{L_n}{L_T} \right)^{1/2}. \tag{A2}$$

Equation (A2) implies that the ITG growth rate has an explicit charge dependence apart from depending on charge and mass through the magnetic and diamagnetic frequencies (or ultimately through the sound speed and Larmor radius). Thus the ITG growth rates in species units are expected to be higher for ions with $Z > 1$.

[1]M. Bessenrodt-Weberpals, F. Wagner, O. Gehre, L. Giannone, J. Hofmann, A. Kallenbach, K. McCormick, V. Mertens, H. Murmann, F. Ryter, B. D. Scott, G. Siller, F. X. Soldner, A. Stabler, K.-H. Steuer, U. Stroth, N. Tsois, H. Verbeek, and H. Zohm, Nucl. Fusion **33**, 1205 (1993).
[2]R. J. Hawryluk, Rev. Mod. Phys. **70**, 537 (1998).
[3]J. Jacquinot and JET Team, Plasma Phys. Controlled Fusion **41**, A13 (1999).
[4]S. Scott, M. Zarnstorff, C. W. Barnes, R. Bell, N. Bretz, C. Bush, Z. Chang, D. Ernst, R. Fonck, L. Johnson, E. Mazzucato, R. Nazikian, S. Paul, J. Schivell, E. J. Synakowski, H. Adler, M. Bell, R. Bundy, E. Fredrickson, B. Grek, A. Janos, D. Johnson, D. McCune, H. Park, A. Ramsey, M. H. Redi, G. Taylor, M. Thompson, and R. Wieland, Phys. Plasmas **2**, 2299 (1995).
[5]J. Q. Dong, W. Horton, and W. Dorland, Phys. Plasmas **1**, 3635 (1994).
[6]G. Bateman, A. Kritz, V. Parail, J. Cordey, and JET Team, Phys. Plasmas **6**, 4607 (1999).
[7]M. Tokar, D. Kalupin, and B. Unterberg, Phys. Rev. Lett. **92**, 215001 (2004).
[8]R. Waltz, Phys. Rev. Lett. **93**, 239501 (2004).
[9]D. Ernst, B. Coppi, S. Scott, M. Porkolab, and T. Group, Phys. Rev. Lett. **81**, 2454 (1998).
[10]J. Candy and R. Waltz, J. Comput. Phys. **186**, 545 (2003).
[11]C. Estrada-Mila, J. Candy, and R. Waltz, Phys. Plasmas **12**, 022305 (2005).
[12]See https://fusion.gat.com/theory/gyro for the technical documentation on GYRO.
[13]J. Candy and E. Belli, General Atomics Technical Report No. GA-A26818, 2010.
[14]T. Fredian and J. Stillerman, Fusion Eng. Des. **60**, 229 (2002).
[15]W. Pfeiffer, R. Davidson, R. Miller, and R. Waltz, General Atomics Technical Report No. GA-A16178, 1980.
[16]See http://w3.pppl.gov/transp for documentation on TRANSP.
[17]R. Hawryluk, *Physics of Plasmas Close to Thermonuclear Conditions*, edited by B. Coppi *et al*. (CEC, Brussels, 1980), pp. 19–46.
[18]E. Belli and J. Candy, Plasma Phys. Controlled Fusion **51**, 075018 (2009).
[19]J. Candy, Plasma Phys. Controlled Fusion **51**, 105009 (2009).
[20]F. Romanelli and S. Briguglio, Phys. Fluids B **2**, 754 (1990).
[21]E. Belli and J. Candy, Phys. Plasmas **17**, 112314 (2010).
[22]H. Sugama and W. Horton, Phys. Plasmas **5**, 2560 (1998).
[23]C. Holland, L. Schmitz, T. Rhodes, W. Peebles, J. Hillesheim, G. Wang, L. Zeng, E. Doyle, S. Smith, R. Prater, K. H. Burrell, J. Candy, R. E. Waltz, J. E. Kinsey, G. M. Staebler, J. C. DeBoo, C. C. Petty, G. R. McKee, Z. Yan, and A. E. White, Phys. Plasmas **18**, 056113 (2011).
[24]M. Kotschenreuther, W. Dorland, M. A. Beer, and G. W. Hammett, Phys. Plasmas **2**, 2381 (1995).
[25]J. Candy, C. Holland, R. Waltz, M. Fahey, and E. Belli, Phys. Plasmas **16**, 060704 (2009).
[26]G. Staebler, J. Kinsey, and R. Waltz, Phys. Plasmas **14**, 055909 (2007).
[27]G. Staebler and J. Kinsey, Phys. Plasmas **17**, 122309 (2010).
[28]C. Holland, A. E. White, G. R. McKee, M. W. Shafer, J. Candy, R. E. Waltz, L. Schmitz, and G. R. Tynan, Phys. Plasmas **16**, 052301 (2009).